Proceedings of the ASME 2022
International Mechanical Engineering Congress and Exposition
IMECE2022
October 30–November 3, 2022, Columbus, OH

IMECE2022-90385

AN EVOLUTIONARY AEROELASTIC DESIGN APPROACH FOR SPARS AND RIBS OF FLYING WING AIRCRAFT

Mojtaba Moshtaghzadeh[1], Natalia Rangel[1], Adrian Bejan[2], Pezhman Mardanpour[1,*]

[1]Florida International University, Miami, FL
[2]Duke University, Durham, NC

ABSTRACT

The purpose of this paper is to examine how rib configurations and spar configurations influence flying wing stability. Flying wing aircraft exhibit enhanced flutter characteristics when stresses flow smoothly through the wing. We prevent stress strangulation through spar cross-sections by changing the configuration in the plunge direction. We employ and develop computer programs Gmsh, Variational Asymptotic Beam Sectional Analysis, MATLAB scripts, and Nonlinear Aeroelastic Trim and Stability of High Altitude Long Endurance Aircraft. The configurations are designed by considering the same material, mass, and flight conditions. The results indicate that the design with the smoother stress distribution through the wing has a higher flutter speed. It is shown that the σ_{11} and Von-Misses stress distributions have an important effect on the stability of a flying wing aircraft.

Keywords: Evolutionary design, Constructal law, Rib and spar configuration, Flutter, Flying wing aircraft

NOMENCLATURE

c	Chord
a	Deformed beam aerodynamic frame of reference
B	Deformed beam cross-sectional frame of reference
b	Undeformed beam cross-sectional frame of reference
$\mathbf{b}_i$	Unit vectors in undeformed beam cross-sectional frame of reference ($i = 1, 2, 3$)
$\mathbf{B}_i$	Unit vectors of deformed beam cross-sectional frame of reference ($i = 1, 2, 3$)
C^{ib}	Transformation matrix from the undeformed frame b to inertial frame i
C^{iB}	Transformation matrix from the deformed frame B to inertial frame i
C^{bi}	Transformation matrix from the inertial frame i to deformed frame b
C^{Bi}	Transformation matrix from the inertial frame i to deformed frame B
c_{l_0}, c_{d_0}	Aerodynamic lift and drag coefficients at zero angle of attack
f	Column matrix of internal force measured in $\mathbf{B}_i$ basis
F	bulk value
$c_{l\beta}$	Lift coefficient w.r.t. flap deflection (β)
$c_{l\alpha}$	Lift coefficient w.r.t. angle of attack (α)
$c_{m\beta}$	Pitch moment coefficient w.r.t. flap deflection (β)
e	Column matrix of distributed, applied force measured in $\mathbf{B}_i$ basis
e_1	Offset of aerodynamic center from the origin of frame of reference along $\mathbf{b}_2$
H	Column matrix of cross-sectional angular momentum measured in $\mathbf{B}_i$ basis
$\mathbf{g}$	Gravitational vector in $\mathbf{B}_i$ basis
i	Inertial frame of reference
$\mathbf{i}_i$	Unit vectors for inertial frame of reference ($i = 1, 2, 3$)
k	Column matrix of undeformed beam initial curvature and twist measured in $\mathbf{b}_i$ basis
I	Cross-sectional inertia matrix
u	Column matrix of displacement vector measured in $\mathbf{b}_i$ basis
m	Column matrix of distributed, applied moment measured in $\mathbf{B}_i$ basis
P	Column matrix of cross-sectional linear momentum measured in $\mathbf{B}_i$ basis
M	Column matrix of internal moment measured in $\mathbf{B}_i$ basis
r	Column matrix of position vector measured in $\mathbf{b}_i$ basis
V	Column matrix of velocity measured in $\mathbf{B}_i$ basis
K	Column matrix of deformed beam curvature and twist measured in $\mathbf{B}_i$ basis
β	Trailing edge flap angle
x_1	Axial coordinate of beam
α	Angle of attack
γ	Column matrix of 1D generalized force strain measures
κ	Column matrix of elastic twist and curvature measures (1D generalized moment strain measures)
Δ	Identity matrix

*Corresponding author: Pezhman.Mardanpour@fiu.edu
Documentation for `asmeconf.cls`: Version 1.30, August 3, 2022.

Ω	Column matrix of cross-sectional angular velocity
μ	Mass per unit length
λ	Column matrix of induced flow states
ρ	Air density
ξ	Column matrix of center of mass offset from the frame of reference origin
ψ	Column matrix of small incremental rotations
$\hat{(\,)}$	Nodal variable
$\dot{(\,)}$	Partial derivative with respect to time
$(\,)'$	Partial derivative with respect to x_1

1. INTRODUCTION

The need for accessible, reliable and more efficient flight has increased rapidly over the past decades. The search for an aircraft that can fly faster and safely is pushing for innovative ways of design.

From conventional design procedures of trial an error to simulation, there were considerable benefits in cost and cycle time reduction [1]. Moving into optimization, with classical and traditional methods for reducing weight and increasing efficiency, then size, shape and topology optimization [2–4] allowed for a more holistic approach into the design of aircraft components. However, these methods still present many limitations and require several iterations and the setting of very clear boundary conditions for them to work accurately, as pointed out in Ref. [4].

With the introduction of constructal law we turn into an evolutionary approach to design. The constructal principle states that "For a finite-size flow system to persist in time (to live), its configuration must evolve freely in such a way that provides greater and greater access to the currents that flow through it" [5]. This approach was inspired by design in nature, Bejan et al. [6] that by following this principle the aircraft design is more efficient and is united with birds and other animals. By searching for this principle and applying it to the way we design and build, it has been discovered that the correlation with better flow of energy and efficiency is present all around us [7].

In the case of aircraft design, we see the use constructal law for the purpose of stability and speed. The aeroelasticity properties of the aircraft from the lens of the flow of stresses had been considered as a function for design. In doing this, we take predictive approach instead of reactive, by moving away from configurations that have the highest stress strangulation into the ones that allow for a better flow access [8–10].

This approach has been successful in predicting the best configuration for a particular design in the previous studies. Mardanpour et al. [8] studied the engine placement and flow of stress in the wing and explored that the maximum flutter speed is achieved with the configuration that has the least stress strangulation. In contrast, the lowest flutter speed is found with the highest stress strangulation. Izadpanahi et al. [9] compared curved vs. swept wing configurations and discovered a relation between higher flutter speed and better stress flow in swept wings. This pattern is also found in Ref. [10] when the inflected wings and their flow of stresses were studied. In this case the inflected wing with the lowest stress strangulation had the better stability and highest flutter speed.

Looking further into the wing configuration, we move away from the wing shape and curvature into the wing internal components, composed mainly of the ribs, spars and stringers. The ribs are a critical component of the wing, which their size and weight are highly depending on their position on the wing in the spanwise direction. As they are located closer to the root, they must bear significant loads from the engines and thrust [11].

Furthermore, the wing has another critical component worth the analysis; the spars and stringers. The spars have the function of bearing the transversal shear and spanwise bending [12]. There have been several studies on the analysis of structure and strength per unit of weight to increase the efficiency of this compononet of the wing [13–17]. Girennavar et al. [15] investigated the design of a wing spar using a method of optimization to find the minimum weight allowed for a certain configuration. They used an iterative process and find the highest stress point in their configurations to reach to the most efficient design using Finite Element Analysis. Ajith et al. [17] compared the spar design was conducted with two approaches; the conventional spar design based on the strength of material approach and an optimized design using iterative method and optimization.

Grbović et al. [16] used shape optimization for the spar analysis. They focused on finding the most fatigue resistant configuration using a method called "W/I". The "W/I" method is also used again by Chinni et al. [13] to find a design which is resistance to fatigue and the critical load of a small airplane. They employed the approach of strength of materials to determine the size shape and composition of the two-spar configuration and spar web. Although these studies provided an optimized design with an acceptable strength, weight and fatigue resistance, they did not considered how the spar and rib configurations affect the aeroleastic stability of the aircraft. Moshtaghzadeh et al. et al. [18] discovered that the cross-section configuration of the wing, specifically the cross-section design of the ribs, have a significant effect on stability and flutter speed. They proposed several cross-section configurations using different shapes in the lead-lag and plunge directions to configure the ribs for a particular airfoil. They presented the flow of stress through the cross-sections and aircraft. It is discovered that the constructal law principle prevails with observing the stress distribution in cross-sections. It is discovered that the better stability and higher flutter speed is associated with the configuration that benefits the most the flow of stresses and reduces the stress strangulation.

A flying wing aircraft's stability and flow of stresses are investigated in this paper by examining its wing spar configuration. A smoother stress flow and a more stable cross-section configuration are sought. In this work, the aircraft is considered as an elastic body which is subjected to aerodynamic loads. We find the flutter characteristic of a flying wing aircraft with three different spar configurations. Then, we observe how the stress distribution is distributed across the cross-sections under the same operating conditions. It is investigated in three directions how stresses flow.

2. THEORY

This section provides the theories behind the NATASHA code and used software in this paper. The details of this section are illustrated in Ref. [18].

2.1 Nonlinear Composite Beam Theory

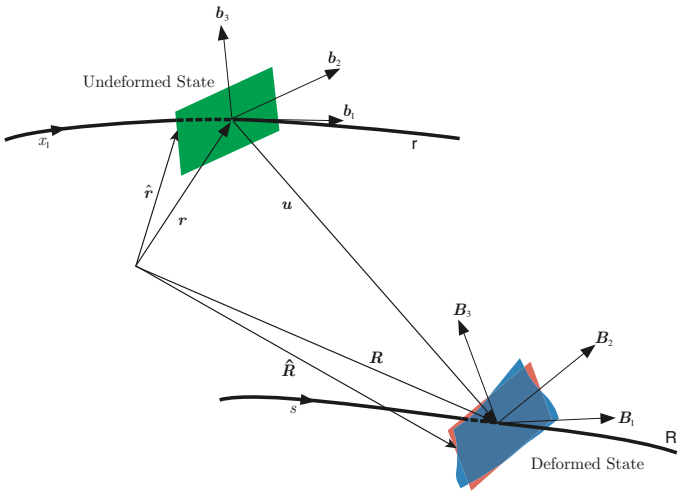

FIGURE 1: SCHEMATIC OF BEAM DEFORMATION [19].

The fully intrinsic nonlinear composite beam theory is founded on the beam's first-order partial differential equations of motion, which have been regardless of displacement and rotation. Variables in the equations are stated in terms of the deformed and undeformed beams' bases of reference frames, $B(x_1, t)$ and $b(x_1)$. These frames are shown in Figure 1. These equations use second-order nonlinearities and are dependent on force, angular velocity, velocity, and moment. The following are the motion equations:

$$\begin{aligned} F_B' + \widetilde{K}_B F_B + f_B &= \dot{P}_B + \widetilde{\Omega}_B P_B \\ M_B' + \widetilde{K}_B M_B + (\widetilde{e}_1 + \widetilde{\gamma}) F_B + m_B &= \dot{H}_B + \widetilde{\Omega}_B H_B + \widetilde{V}_B P_B \end{aligned} \tag{1}$$

The structural constitutive equations relate generalized velocities and strains to moments and stress resultants.

$$\begin{Bmatrix} \gamma \\ \kappa \end{Bmatrix} = \begin{bmatrix} R & S \\ S^T & T \end{bmatrix} \begin{Bmatrix} F_B \\ M_B \end{Bmatrix} \tag{2}$$

The following equation is the inertial constitutive equations [18]

$$\begin{Bmatrix} P_B \\ H_B \end{Bmatrix} = \begin{bmatrix} \mu\Delta & -\mu\widetilde{\xi} \\ \mu\widetilde{\xi} & I \end{bmatrix} \begin{Bmatrix} V_B \\ \Omega_B \end{Bmatrix}. \tag{3}$$

Furthermore, the intrinsic kinematical partial differential equations [19] are derived using strain- and velocity-displacement equations [18].

$$\begin{aligned} V_B' + \widetilde{K}_B V_B + (\widetilde{e}_1 + \widetilde{\gamma})\Omega_B &= \dot{\gamma} \\ \Omega_B' + \widetilde{K}_B \Omega_B &= \dot{\kappa} \end{aligned} \tag{4}$$

The equations are explained in detail in Ref. [20]. This is a full set of partial differential equations in the first order. In terms of velocity (VB), force (FB), moment (MB), and angular velocity ($OmegaB$), 12 boundary conditions are required. Singularities generated by finite rotations are eliminated since the maximum degree of nonlinearities is two, and displacement and rotation variables do not present. In the post-processing procedures, the position and orientation of each elements can be determined if desired.

$$\begin{aligned} r_i' &= C^{ib} e_1 \\ r_i + u_i' &= C^{iB}(e_1 + \gamma) \end{aligned} \tag{5}$$

and

$$\begin{aligned} (C^{bi})' &= -\widetilde{k} C^{bi} \\ (C^{Bi})' &= -(\widetilde{k} + \widetilde{\kappa}) C^{Bi} \end{aligned} \tag{6}$$

2.2 Variational Asymptotic Beam Sectional Analysis (VABS)

Reference [21] used Berdichevsky's Variational Asymptotic Method (VAM) [22] to simplify a three-dimensional elastic problem to a one-dimensional formulation. VAM locates a function's stationary point with one or more minor parameters. It's the best tool for reducing the dimensions of objects like beams, plates, and shells. The Hamilton extended principle and this mathematical method conclude Hodges's geometrically-exact nonlinear composite beam theory [20, 21].

VABS [21, 23, 24] is a software package that simplifies a 3D nonlinear analysis using the variational method. It converts three-dimensional (3D) slender objects into two-dimensional (2D) cross-sections and one-dimensional (1D) beam analyses. VABS reduces computational costs from hours to seconds while preserving detailed 3D FEA reliability. It calculates cross-sectional properties using a finite element mesh of the cross-section and material parameters as inputs (e.g., inertial and structural properties). Stress recovery is also accomplished using inputs such as axial and shear forces, moments, and distributed forces (applied and inertial)[9].

2.3 Finite State Induced Model

The published studies [25–27]demonstrate that The two-dimensional finite state aerodynamic model of Peters et al. [25] is an acceptable representation of aerodynamic loads occurring on high-aspect ratio wings. At the quarter-chord, the drag, lift, and pitching moment are given by the following equations. The detail of this model is explained in Ref. [18].

$$\begin{aligned} L_{aero} = \rho b[(c_{l_0} + c_{l_\beta}\beta)V_T V_{a_2} - c_{l_\alpha}\dot{V}_{a_3}\, b/2 - c_{l_\alpha} V_{a_2}(V_{a_3} + \lambda_0 - \\ \Omega_{a_1} b/2) - c_{d_o} V_T V_{a_3}] \end{aligned} \tag{7}$$

$$\begin{aligned} D_{aero} = \rho b[-(c_{l_0} + c_{l_\beta}\beta)V_T V_{a_3} + c_{l_\alpha}(V_{a_3} + \lambda_0)^2 - \\ c_{d_o} V_T V_{a_2}] \end{aligned} \tag{8}$$

$$\begin{aligned} M_{aero} = 2\rho b[(c_{m_0} + c_{m_\beta}\beta)V_T - c_{m_\alpha} V_T V_{a_3} - b c_{l_\alpha}/8 V_{a_2}\Omega_{a_1} - \\ b^2 c_{l_\alpha}\dot{\Omega}_{a_1}/32 + b c_{l_\alpha}\dot{V}_{a_3}/8] \end{aligned} \tag{9}$$

$$V_T = (V_{a_2}^2 + V_{a_3}^2)^{1/2}. \tag{10}$$

$$\sin\alpha = \frac{-V_{a_3}}{V_T} \tag{11}$$

$$\alpha_{rot} = \frac{\Omega_{a_1} b/2}{V_T} \tag{12}$$

$$[A_{\text{induced flow}}]\{\dot{\lambda}\} + \left(\frac{V_T}{b}\right)\{\lambda\} = \left(-\dot{V}_{a_3} + \frac{b}{2}\dot{\Omega}_{a_1}\right)\{c_{\text{induced flow}}\} \tag{13}$$

$$\lambda_0 = \frac{1}{2}\left\{b_{induced\ flow}\right\}^T \{\lambda\} \tag{14}$$

where λ is the column matrix of induced flow states, and $\left[A_{induced\ flow}\right], \left\{b_{induced\ flow}\right\}, \left\{c_{induced\ flow}\right\}$ are constant matrices and they are found in Ref.[25] [8].

2.4 Aeroelastic System

By combining the aerodynamic and structural equations, the aeroelastic system is characterized as:

$$[A]\{\dot{x}\} + \{B(x)\} = \{f_{cont}\} \tag{15}$$

f_{cont} and $\{x\}$ are the vector of the flight controls and the vector of all the aeroelastic variables. The nonlinear ordinary differential equations emerging from this process are linearized around a static equilibrium state. The linearized system looks like this [18]:

$$[A]\left\{\dot{\hat{x}}\right\} + [B]\left\{\hat{x}\right\} = \left\{\hat{f}_{\ cont}\right\} \tag{16}$$

Nonlinear algebraic equations determine the equilibrium state, which the code Nonlinear Aeroelastic Trim and Stability of HALE Aircraft (NATASHA) [28, 29] solves using the Newton-Raphson approach [28]to find the trim solution. This computer package is based on the finite induced flow model of Peters et al. [25] and Hodges' nonlinear composite beam theory [19].and Peters et alfinite .'s induced flow model. Both experimental and numerical benchmarks have been used to verify and validate NATASHA [26, 27, 30–36].

3. NUMERICAL SIMULATION

Gmsh [37], VABS, and NATASHA are the three computer programs used in this study. Multiple scripts and functions are created in MATLAB to link the software. Scripts and VABS are used to perform stress recovery, as illustrated in Ref. [9, 38]. We employ Gmsh to discretize each cross-section. The elements' information is imported into VABS software to find the mechanical properties of each cross-section. The obtained properties are then applied to NATASHA to find out the aeroelastic characteristic of flying wings. The VABS software uses the results to determine the stresses in the aircraft.

We analyze the stability of an aircraft with two wings that are each 15 m long. There are 18 elements in each wing, including four ribs and 14 spars. The ribs are 0.25 m long, and the spars are distributed from the fuselage to the tip of the wings. From the center of the fuselage to the root of each wing, the fuselage length is assumed to be 4 meters. We design the spar and rib configurations using NACA0012 airfoil with a chord of 1 m. This flying wing aircraft design contains two engines with 10 kg weight. The ailerons are located between the tip and mid-span of wings. The wings are swept with an angle of 15^o. Figure 2 presents the location of spar and ribs through the aircraft.

Figure 2 shows the spar and ribs configurations. Ref. [18] compared different cross-section configurations and concluded that the oval hollows arrangement has the highest stability. The oval configuration in Figure 3 is assigned to the rib cross-sections. In Table 1, we show the mechanical properties of spar configurations. A detailed description of the mechanical properties of rib cross-sections is given in Ref. [18]. In addition, Table 2 presents the aerodynamic coefficient and properties in this stability analysis.

4. RESULTS AND DISCUSSION

The purpose of this section is to discuss the flutter characteristic and to explain how stress distribution and aircraft stability are related.

Table 3 presents the flutter speed and frequency of these proposed designs. The rib configurations are considered same in all cases. The same material properties are utilized, and mass is constant in all spar configurations. Thickness of branches in the plunge direction is increased from case I to case III. The results indicate that the cross-sectional configuration of the aircraft can significantly affect its stability. Among these configurations, design III has the highest flutter instability with a speed of 49.63 m/s. The results illustrate that the substituting mass from the plunge direction ($\mathbf{b}_3$) to the lead-lag direction ($\mathbf{b}_2$) improves the flutter instability. Existing voids in the plunge direction of spars has an advantage for the stability of the aircraft.

Figures 4 - 10 depict how the stresses are distributed through the spar and rib cross-sections and aircraft. The stresses are obtained based on the cruise speed of 35 m/s and the same flight condition. Figure 4 presents σ_{11} distribution through the closed spar cross-section to the fuselage. It is found that the lower region of the cross-section is under tension and the upper region of the cross-section is under compression. As the design varies from case I to case III, the stress is distributed in the b_3 direction with a smoother distribution.

σ_{12} and σ_{13} distributions are shown in Figures 5 and 6. It is shown that the stress magnitudes in these two directions are decreased in comparison with σ_{11}. In conclusion, σ_{12} and σ_{13} have less influence on the stability of the aircraft. Figure 7 shows how the Von-Mises stress distributes through the spar cross-sections. Although the cross-section's skin experiences significant stress, it is demonstrated that the connections in the plunge direction reduce the stress strangulation in the cross-section's skin. The Von-Misses stress has the lowest value in case III, which is associated with the highest flutter speed.

Figures 8- 10 depict the Von-Mises how stresses flow through the designed aircraft wing. It is found that maximum stress occurs at the outer region of spar and rib cross-sections. A substantial amount of stress strangulation is observed at the root of the wing. From the root to the tip of the wing, this phenomenon decreases. However, the majority of stresses travel in a lead-lag direction; branches in a plunge direction facilitate a smoother flow of stress. Compared to spars, ribs experience a much smaller magnitude of stress. Case III has the lowest and smoothest stress distribution, which could enhance the stability of the design.

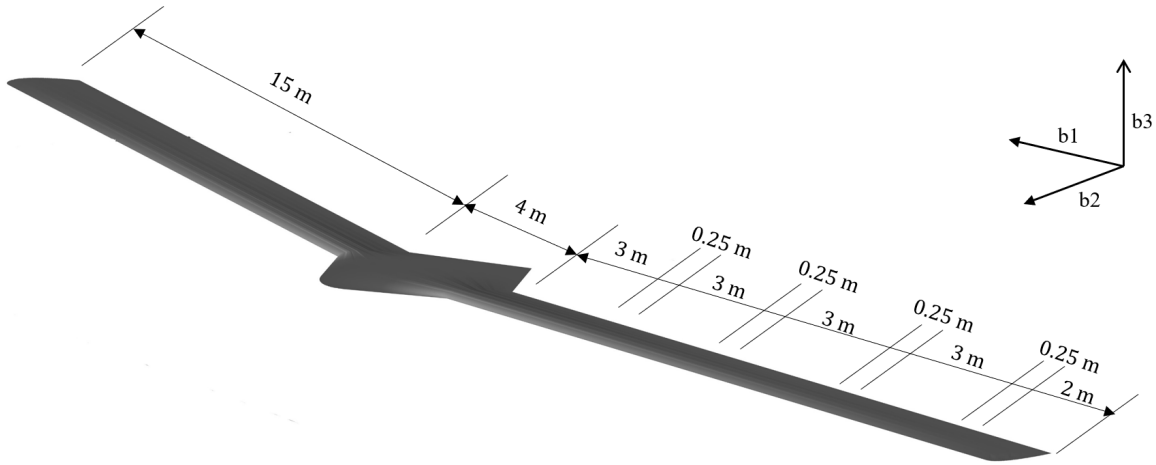

FIGURE 2: SCHEMATIC VIEW OF THE FLYING WING AIRCRAFT.

TABLE 1: THE SPAR CROSS SECTIONAL PROPERTIES IN SI UNIT SYSTEM; CASES I, II, AND III.

Property	Case I	Case II	Case III
Span $[m]$	15	15	15
S $[N^{-1}.m^{-1}]$	$\begin{bmatrix} 0 & -1.61\times10^{-15} & 3.57\times10^{-9} \\ -6.84\times10^{-15} & 0 & 0 \\ -5.66\times10^{-7} & 0 & 0 \end{bmatrix}$	$\begin{bmatrix} 0 & -4.15\times10^{-14} & 3.54\times10^{-9} \\ 6.04\times10^{-13} & 0 & 0 \\ -5.66\times10^{-7} & 0 & 0 \end{bmatrix}$	$\begin{bmatrix} 0 & -1.54\times10^{-15} & 3.56\times10^{-9} \\ -1.04\times10^{-15} & 0 & 0 \\ -5.59\times10^{-6} & 0 & 0 \end{bmatrix}$
R $[N^{-1}]$	$\begin{bmatrix} 8.015\times10^{-9} & 0 & 0 \\ 0 & 3.09\times10^{-8} & -1.75\times10^{-14} \\ 0 & -1.75\times10^{-14} & 2.89\times10^{-7} \end{bmatrix}$	$\begin{bmatrix} 8.0\times10^{-9} & 0 & 0 \\ 0 & 3.07\times10^{-8} & 5.78\times10^{-13} \\ 0 & 5.78\times10^{-13} & 2.86\times10^{-7} \end{bmatrix}$	$\begin{bmatrix} 8.02\times10^{-9} & 0 & 0 \\ 0 & 3.05\times10^{-8} & -1.73\times10^{-14} \\ 0 & -1.73\times10^{-14} & 2.83\times10^{-7} \end{bmatrix}$
T $[N^{-1}.m^{-2}]$	$\begin{bmatrix} 4.11\times10^{-6} & 0 & 0 \\ 0 & 5.53\times10^{-6} & -4.92\times10^{-14} \\ 0 & -4.92\times10^{-14} & 1.04\times10^{-7} \end{bmatrix}$	$\begin{bmatrix} 4.13\times10^{-6} & 0 & 0 \\ 0 & 5.47\times10^{-6} & -1.02\times10^{-12} \\ 0 & -1.02\times10^{-12} & 1.04\times10^{-7} \end{bmatrix}$	$\begin{bmatrix} 4.06\times10^{-6} & 0 & 0 \\ 0 & 5.46\times10^{-6} & -4.78\times10^{-14} \\ 0 & -4.78\times10^{-14} & 1.04\times10^{-8} \end{bmatrix}$
I $[kg.m]$	$\begin{bmatrix} 1.99\times10^{-1} & 0 & 0 \\ 0 & 3.631\times10^{-3} & 7.0w\times10^{-15} \\ 0 & 7.02\times10^{-15} & 1.96\times10^{-1} \end{bmatrix}$	$\begin{bmatrix} 1.99\times10^{-1} & 0 & 0 \\ 0 & 3.68\times10^{-3} & -1.63\times10^{-13} \\ 0 & -1.63\times10^{-13} & 1.95\times10^{-1} \end{bmatrix}$	$\begin{bmatrix} 1.99\times10^{-1} & 0 & 0 \\ 0 & 3.68\times10^{-3} & -7.03\times10^{-15} \\ 0 & -7.03\times10^{-15} & 1.95\times10^{-1} \end{bmatrix}$
ξ $[m]$	$\begin{bmatrix} 0 \\ 4.06\times10^{-2} \\ 1.16\times10^{-19} \end{bmatrix}$	$\begin{bmatrix} 0 \\ 4.03\times10^{-2} \\ -7.24\times10^{-20} \end{bmatrix}$	$\begin{bmatrix} 0 \\ 4.05\times10^{-2} \\ -1.85\times10^{-19} \end{bmatrix}$
Mass $[kg.m^{-1}]$	2.57	2.57	2.57
Chord $[m]$	1	1	1

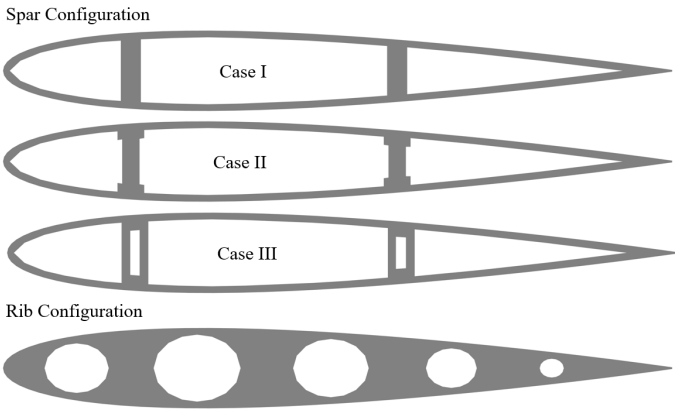

FIGURE 3: RIB AND SPAR CROSS-SECTION CONFIGURATIONS.

TABLE 2: THE AERODYNAMIC COEFFICIENTS AND PROPERTIES.

Property	$\rho\ [kg.m^{-3}]$	c_{l_β}	c_{l_α}	c_{m_0}	c_{d_0}	c_{m_α}	c_{m_β}	e [m]
Value	0.0889	1	2π	0.0	0.01	-0.08	-0.25	0.25

TABLE 3: FLUTTER SPEED AND RELATED FREQUENCY.

Case	Flutter [m/s]	Frequency [rad/s]
I	49.37	6.59
II	49.53	6.62
III	49.68	6.63

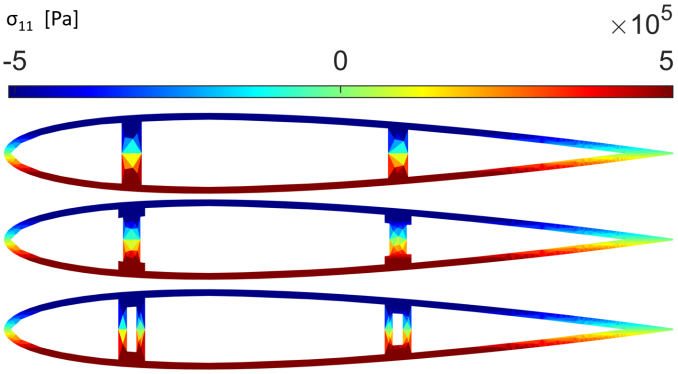

FIGURE 4: σ_{11} STRESS DISTRIBUTION IN SPAR CROSS-SECTION.

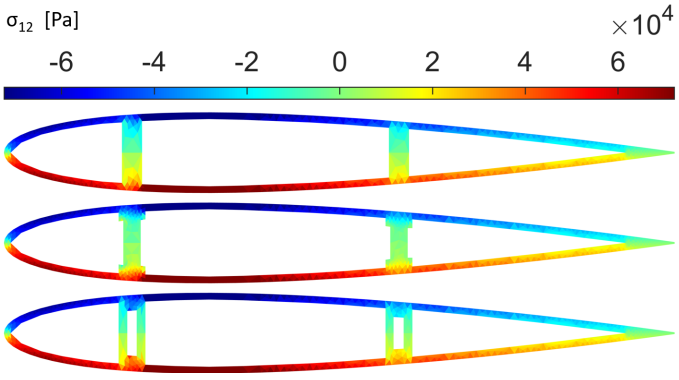

FIGURE 5: σ_{12} STRESS DISTRIBUTION IN SPAR CROSS-SECTION.

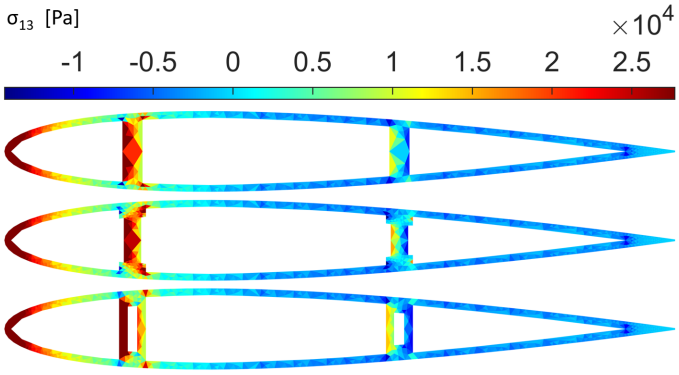

FIGURE 6: σ_{13} STRESS DISTRIBUTION IN SPAR CROSS-SECTION.

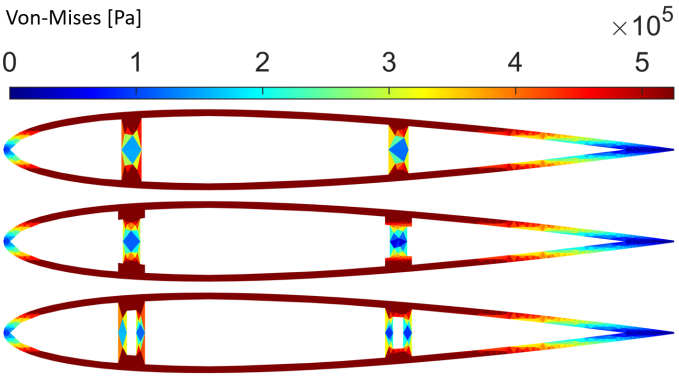

FIGURE 7: VON-MISES STRESS DISTRIBUTION IN SPAR CROSS-SECTION.

5. CONCLUSION

By varying the configuration of the ribs, we demonstrated how flying wings change their stability. The Constructal law and the idea of flow of stresses were used to examine the aeroelastic stability of the three rib configuration designs of a flying wing aircraft in this study.

The results illustrate that the Von-Mises and σ_{11} stresses strongly impact the stability of a flying wing aircraft. The most stress-carrying direction is the lead-lag direction. As a result of the existing strips in the plunge direction, the aircraft could be stabilized more effectively. Adding mass to the lead-lag direction instead of the plunge direction smooths out the stress distribution. In addition, it prevents stress strangulation through the cross-section, resulting in higher flutter speed.

Comparing these proposed designs indicates that when the stress flows through the cross-section smoothly, the flutter occurs at a higher speed. The rib configuration with boxes in the plunge direction has the highest flutter speed among all designs.

ACKNOWLEDGMENTS

The U.S. National Science Foundation (NSF) supports Professor Mardanpour's research under grant 1934749.

REFERENCES

[1] Rao, JS. "Advances in aero structures." *Procedia Engineering* Vol. 144 (2016): pp. 3–25.

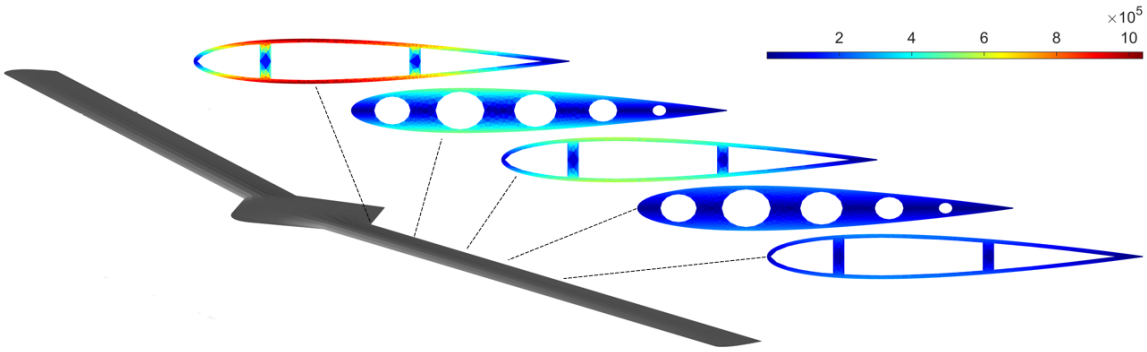

FIGURE 8: VON-MISES STRESS DISTRIBUTION THROUGH THE WING OF AIRCRAFT I.

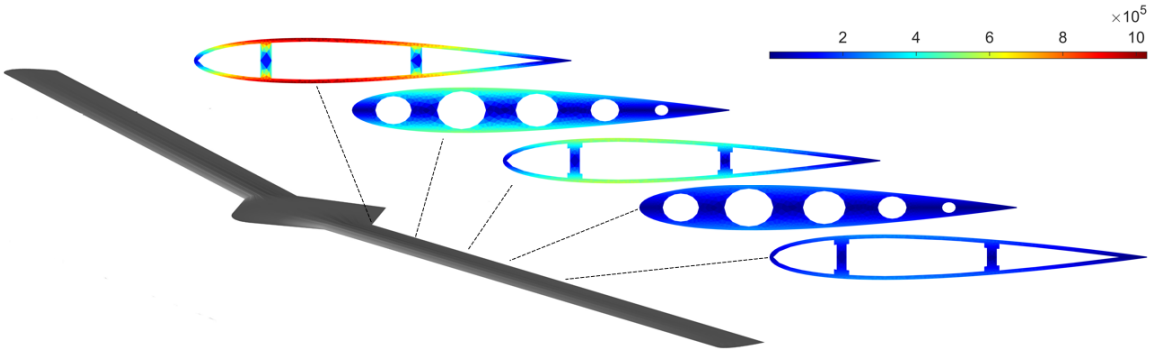

FIGURE 9: VON-MISES STRESS DISTRIBUTION THROUGH THE WING OF AIRCRAFT II.

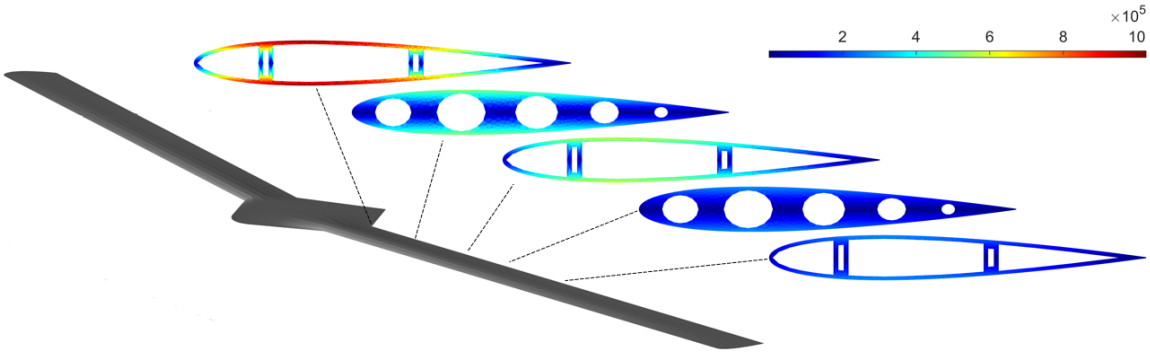

FIGURE 10: VON-MISES STRESS DISTRIBUTION THROUGH THE WING OF AIRCRAFT III.

[2] Krog, Lars, Tucker, Alastair, Kemp, Martin and Boyd, Richard. "Topology optimisation of aircraft wing box ribs." *10th AIAA/ISSMO multidisciplinary analysis and optimization conference*: p. 4481. 2004.

[3] Schuhmacher, Gerd, Murra, Ibrahim, Wang, Liu, Laxander, Armin, O'Leary, Owen and Herold, Michael. "Multidisciplinary design optimization of a regional aircraft wing box." *9th AIAA/ISSMO Symposium on Multidisciplinary Analysis and Optimization*: p. 5406. 2002.

[4] Krog, Lars, Tucker, Alastair, Rollema, Gerrit et al. "Application of topology, sizing and shape optimization methods to optimal design of aircraft components." *Proc. 3rd Altair UK HyperWorks users conference*. 2002.

[5] Bejan, Adrian and Lorente, Sylvie. "Constructal law of design and evolution: Physics, biology, technology, and society." *Journal of Applied Physics* Vol. 113 No. 15 (2013): pp. –. DOI 10.1063/1.4798429.

[6] Bejan, Adrian, Charles, JD and Lorente, Sylvie. "The evolution of airplanes." *Journal of Applied Physics* Vol. 116 No. 4 (2014): p. 044901.

[7] Bejan, Adrian. "The constructal law of organization in nature: tree-shaped flows and body size." *Journal of Experimental Biology* Vol. 208 No. 9 (2005): pp. 1677–1686.

[8] Mardanpour, Pezhman, Izadpanahi, Ehsan, Rastkar, Siavash, Lorente, Sylvie and Bejan, Adrian. "Constructal Design of Aircraft: Flow of Stresses and Aeroelastic Stability." *AIAA Journal* Vol. 57 No. 10 (2019): pp. 4393–4405.

[9] Izadpanahi, Ehsan, Rastkar, Siavash and Mardanpour, Pezhman. "Constructal Design of Flying Wing Aircraft: Curved and Swept Configurations." *AIAA Journal* Vol. 57 No. 12 (2019): pp. 5527–5542.

[10] Mardanpour, Pezhman, Izadpanahi, Ehsan, Powell, Shanae, Rastkar, Siavash and Bejan, Adrian. "Inflected wings in flight: Uniform flow of stresses makes strong and light wings for stable flight." *Journal of Theoretical Biology* Vol. 508 (2021): p. 110452.

[11] Megson, Thomas Henry Gordon. *Introduction to aircraft structural analysis*. Butterworth-Heinemann (2013).

[12] Kaur, Ramandeep and Ambri, A. "Spars and stringers-function and designing." *Int. J. Aerosp. Mech. Eng* Vol. 1 No. 1 (2014): pp. 58–61.

[13] Chinni, Bala Naga Bharath and Siddappa, PN. "Design and analysis of front spar wing-tip segment for a small transport aircraft." *Materials Today: Proceedings* Vol. 52 (2022): pp. 1846–1851.

[14] Peruru, Sivarama Prasad and Abbisetti, Suman Babu. "Design and finite element analysis of aircraft wing using ribs and spars." *Int. Res. J. Eng. Technol.(IRJET)* Vol. 4 No. 06 (2017): pp. 2133–2139.

[15] Girennavar, Mutturaj, Soumya, H, Subodh, H, Heraje, Tanvi J and PY, Deepak Raj. "Design, Analysis and Testing of Wing Spar for Optimum Weight." *International Journal of Research and Scientific Innovation (IJRSI)* Vol. 4 No. VII (2017): pp. 104–112.

[16] Grbović, Aleksandar, Kastratović, Gordana, Sedmak, Aleksandar, Eldweib, Khalid and Kirin, Snezana. "Determination of optimum wing spar cross section for maximum fatigue life." *International Journal of Fatigue* Vol. 127 (2019): pp. 305–311.

[17] Ajith, VS, Paramasivam, Ravikumar and Vidhya, K. "Study of optimal design of spar beam for the wing of an aircraft." *International Journal of Engineering Development and Research* Vol. 5 No. 3 (2017): pp. 179–193.

[18] Moshtaghzadeh, Mojtaba, Izadpanahi, Ehsan, Bejan, Adrian and Mardanpour, Pezhman. "Evolutionary Aeroelastic Design of Flying-Wing Cross Section." *AIAA Journal* Vol. 60 No. 2 (2022): pp. 913–924.

[19] Hodges, Dewey H. "Geometrically exact, intrinsic theory for dynamics of curved and twisted anisotropic beams." *AIAA journal* Vol. 41 No. 6 (2003): pp. 1131–1137. DOI 10.2514/2.2054.

[20] Hodges, Dewey H. "Nonlinear composite beam theory." *Progress in astronautics and aeronautics* Vol. 213 (2006): p. 304.

[21] Yu, Wenbin, Hodges, Dewey H and Ho, Jimmy C. "Variational asymptotic beam sectional analysis–an updated version." *International Journal of Engineering Science* Vol. 59 (2012): pp. 40–64.

[22] Berdichevskii, VL. "Variational-asymptotic method of constructing a theory of shells: PMM vol. 43, no. 4, 1979, pp. 664–687." *Journal of Applied Mathematics and Mechanics* Vol. 43 No. 4 (1979): pp. 711–736.

[23] Yu, Wenbin, Volovoi, Vitali V, Hodges, Dewey H and Hong, Xianyu. "Validation of the variational asymptotic beam sectional analysis." *AIAA journal* Vol. 40 No. 10 (2002): pp. 2105–2112.

[24] Yu, Wenbin and Hodges, Dewey H. "Generalized Timoshenko theory of the variational asymptotic beam sectional analysis." *Journal of the American Helicopter Society* Vol. 50 No. 1 (2005): pp. 46–55.

[25] Peters, David A, Karunamoorthy, Swaminathan and Cao, Wen-Ming. "Finite state induced flow models. I-Two-dimensional thin airfoil." *Journal of Aircraft* Vol. 32 No. 2 (1995): pp. 313–322. DOI 10.2514/3.46718.

[26] Sotoudeh, Zahra, Hodges, Dewey H and Chang, Chong-Seok. "Validation studies for aeroelastic trim and stability of highly flexible aircraft." *Journal of Aircraft* Vol. 47 No. 4 (2010): pp. 1240–1247. DOI 10.2514/1.46974.

[27] Goland, Martin and Luke, YL. "The flutter of a uniform wing with tip weights." *Journal of Applied Mechanics* Vol. 15 No. 1 (1948): pp. 13–20.

[28] Patil, Mayuresh J and Hodges, Dewey H. "Flight dynamics of highly flexible flying wings." *Journal of Aircraft* Vol. 43 No. 6 (2006): pp. 1790–1799. DOI 10.2514/1.17640.

[29] Chang, C-S, Hodges, Dewey H and Patil, Mayuresh J. "Flight dynamics of highly flexible aircraft." *Journal of Aircraft* Vol. 45 No. 2 (2008): pp. 538–545. DOI 10.2514/1.30890.

[30] Timoshenko, Stephen P and Gere, James M. "Theory of elastic stability second edition." *McGraw-Hill Book Company: New York* .

[31] Simitses, George J and Hodges, Dewey H. *Fundamentals of structural stability*. Butterworth-Heinemann, Burlington (2006).

[32] Dowell, EH, Traybar, J and Hodges, Dewey H. "An experimental-theoretical correlation study of non-linear bending and torsion deformations of a cantilever beam." *Journal of Sound and Vibration* Vol. 50 No. 4 (1977): pp. 533–544. DOI 10.1016/0022-460X(77)90501-6.

[33] Bauchau, Olivier A and Kang, NK. "A multibody formulation for helicopter structural dynamic analysis." *Journal of the American Helicopter Society* Vol. 38 No. 2 (1993): pp. 3–14. DOI 10.4050/JAHS.38.3.

[34] Bauchau, Olivier A. "Computational schemes for flexible, nonlinear multi-body systems." *Multibody System Dynamics* Vol. 2 No. 2 (1998): pp. 169–225. DOI 10.1023/A:100971081.

[35] Saberi, HA, Khoshlahjeh, M, Ormiston, RA and Rutkowski, MJ. "RCAS overview and application to advanced rotorcraft problems." *4th Decennial Specialists' Conference on Aeromechanics*. 2004.

[36] Mardanpour, Pezhman, Hodges, Dewey H, Neuhart, Ryan and Graybeal, Nathan. "Engine placement effect on nonlinear trim and stability of flying wing aircraft." *Journal of Aircraft* Vol. 50 No. 6 (2013): pp. 1716–1725. DOI 10.2514/1.C031955.

[37] Geuzaine, Christophe and Remacle, Jean-François. "Gmsh: A 3-D finite element mesh generator with built-in pre-and post-processing facilities." *International journal for numerical methods in engineering* Vol. 79 No. 11 (2009): pp. 1309–1331.

[38] Izadpanahi, Ehsan, Moshtaghzadeh, Mojtaba, Radnezhad, Hamid Reza and Mardanpour, Pezhman. "Constructal approach to design of wing cross-section for better flow of stresses." *AIAA Scitech 2020 Forum*: p. 0275. 2020.